

5-20-2024

Joint control of a flying robot and a ground vehicle using leader-follower paradigm

Ayşen Süheyla BAĞBAŞI

Ali Emre TURGUT

Kutluk Bilge ARIKAN

Follow this and additional works at: <https://journals.tubitak.gov.tr/elektrik>



Part of the [Computer Engineering Commons](#), [Computer Sciences Commons](#), and the [Electrical and Computer Engineering Commons](#)

Recommended Citation

BAĞBAŞI, Ayşen Süheyla; TURGUT, Ali Emre; and ARIKAN, Kutluk Bilge (2024) "Joint control of a flying robot and a ground vehicle using leader-follower paradigm," *Turkish Journal of Electrical Engineering and Computer Sciences*: Vol. 32: No. 3, Article 9. <https://doi.org/10.55730/1300-0632.4082>




Available at: <https://journals.tubitak.gov.tr/elektrik/vol32/iss3/9>



This work is licensed under a [Creative Commons Attribution 4.0 International License](#).

This Article is brought to you for free and open access by TÜBİTAK Academic Journals. It has been accepted for inclusion in Turkish Journal of Electrical Engineering and Computer Sciences by an authorized editor of TÜBİTAK Academic Journals. For more information, please contact pinar.dundar@tubitak.gov.tr.

Joint control of a flying robot and a ground vehicle using leader-follower paradigm

Ayşen Süheyla BAĞBAŞI^{1,*}, Ali Emre TURGUT², Kutluk Bilge ARIKAN³

¹Mechatronics Engineering Graduate Program, Graduate Institute, TED University, Ankara, Türkiye

²Department of Mechanical Engineering, Faculty of Engineering,
Middle East Technical University, Ankara, Türkiye

³Department of Mechanical Engineering, Faculty of Engineering, TED University, Ankara, Türkiye

Received: 12.04.2023

Accepted/Published Online: 13.03.2024

Final Version: 20.05.2024

Abstract: In this study, a novel control framework for the collaboration of an aerial robot and a ground vehicle that is connected via a taut tether is proposed. The framework is based on a leader-follower paradigm. The leader follows a desired trajectory while the motion of the follower is controlled by an admittance controller using an extended state observer to estimate the tether force. Additionally, a velocity estimator is also incorporated to accurately assess the leader's velocity. An essential feature of our system is its adaptability, enabling role switching between the robots when needed. Furthermore, the synchronization performance of the robots is evaluated through quantitative analysis using the RMS position error metric and circular variance metric that is used in the mirror game to measure synchronization in human interactions. Similar to human-human interactions, we have observed that robotic agents can effectively guide one another based solely on interaction cues and adapt as needed. Our findings demonstrate the remarkable ability of robots to closely follow each other using a velocity estimation approach, without the reliance on sensors. This work contributes to the field by advancing robotic collaboration capabilities under limited sensor conditions, capitalizing on the inherent sensing capabilities of the robots, and providing a versatile platform for the study of cooperative behaviors in artificial systems.

Key words: Tethered quadcopter, ground robot, haptic interaction, quantitative analysis

1. Introduction

Unmanned aerial vehicles (UAVs) have proven to be valuable in various fields such as surveillance, agriculture, transportation, and inspection. These versatile robots have been equipped with advanced sensors and control systems, greatly enhancing their capabilities. However, UAVs face limitations in terms of flight time and payload capacity, which hinder their full potential. Most of the time, UAVs often follow predefined flight paths using conventional control algorithms such as PID for attitude and altitude control. Some studies explore the use of metaheuristic optimization algorithms to fine-tune these control algorithms for improved performance [1, 2]. Cameras also play a crucial role in enhancing the abilities of UAVs. Researchers have studied the use of three-axis gimbal mounted cameras on mobile platforms to enhance real-time target tracking performance, even in the presence of external disturbances [3]. Additionally, there is a growing interest in collaborative approaches between aerial and ground robots. Aerial robots, with their wide field of view, speed, and compact size, can collaborate with other robots to explore and map environments. Despite the presence of real and commercial solutions in these domains, numerous challenges persist, particularly in the realms of multirobot control and

*Correspondence: asuheyla.bagbasi@tedu.edu.tr

interaction with the environment. Addressing these challenges is not straightforward due to various factors. One primary concern in cooperative approaches is the need for quadcopters to navigate within a group to achieve a common goal while considering the presence of neighboring robots [4]. Additionally, the coordination problem becomes more complicated due to limited sensing capabilities of quadcopters, resulting in less information about the surroundings and neighboring robots. Further complications arise when interacting with the other robots, leading to unknown forces, disturbances, and torques that can potentially destabilize the system. An illustrative scenario that encapsulates these challenges is the cooperative transport of payloads suspended by tethers using multiple quadcopters. In such a scenario, robots must collaborate to transport the load while avoiding collisions and preventing undesired movements of the payload, such as swinging. In recent years, extensive research has been carried out for the transportation of payloads suspended by tethers [5–7]. In [8], the potential use of a flexible tether is explored. However, the limited payload capacity of the quadcopters restricts their ability to carry large or heavy objects. To address this issue, alternatives include increasing the size of a single quadcopter to accommodate powerful motors or creating hexacopters or octocopters with more propellers [9, 10].

Another approach involves employing multiple robots to collectively enhance the system's overall load carrying capacity, enabling the manipulation of larger and heavier loads. In collaborative transportation, common solutions often rely on global approaches, where a designated leader calculates the control actions and then disseminates them to other robots [11]. Alternatively, a distributed control method calculates individual control actions based on the grasping points of the robots on the payload, with a shared common goal among the agents [12]. Approaches such as the one presented in [13] generate dynamically feasible routes for aerial vehicles moving through cluttered known environments to control the swarm. Other methods, exemplified by [14–16], adopt a leader-follower approach in multirobot problems, designating one robot as the leader whose motion defines the bulk movement of the group. The leader then guides the movements of each member within the formation group. However, a significant drawback of these strategies for both single and multirobot approaches is the need for complete knowledge of the entire system's state. Such approaches are limited to indoor applications, where a tracking system can be installed to provide the location of all system objects. Outdoor applications are not feasible due to the absence of a tracking system. In [17], Lupashin et al. present an alternative that does not rely on an external motion capture system. Their research focuses on developing a tethered quadcopter to reduce costs and complexities associated with hover-capable flying vehicles, making the technology more accessible. They design a practical control method that utilizes an unscented Kalman filter (UKF) for estimating tether and vehicle attitude states using a simplified onboard inertial sensor. The vehicle commands a high open-loop thrust to maintain the tether taut, restricting vertical movement, while horizontal movement is controlled by shifting the fixed anchor point. The simplified mathematical model of the tether, ignoring mass and elasticity effects, allows for indirect monitoring of the interaction force on the tether. This study facilitates the tether's further use as a tangible tool to interact with the surroundings, leading to the development of the commercial product.

The tethered solution is gaining increasing interest for physically connecting aerial vehicles to a fixed point or a moving platform. Various perspectives on tethered systems have been explored in the literature, with a focus on taut tether approaches in this study due to their scientific significance. One approach involves using a fixed base station tether, serving as a power line for the robot, particularly in industrial sectors requiring extended uptime [18]. Another approach employs a moving base station, as seen in a study [19], where an electrical cable tether supplies power to increase flight time and prevent undesired movement of the aerial vehicle. In [20–22], stabilization and observer design for tethered quadcopters have been investigated, but their assumptions limit

their effectiveness in realistic scenarios involving aggressive maneuvers or dynamic tether elongation. A taut tether offers benefits such as enhanced flight stability and reliability, especially during challenging maneuvers. Sandino et al. [23] proposed using a tether to improve UAV performance in hover under strong wind conditions. The tether's dynamics impact translational vehicle dynamics, providing robustness to external perturbations, while the tension force introduces challenges in system control. Ground devices control the tether tension and the helicopter is controlled by the LQI method. Subsequent studies by the same authors validated the system through simulations involving wind and additional disturbances, focusing on autonomous landing on a moving platform [24], and landing without GPS in [25].

One solution gaining considerable attention is the tethering aerial vehicles to fixed or moving platforms, such as mobile robots, to enable the transfer of power and information and significantly extend the flight time and payload capabilities of UAV. Numerous studies have delved into tethered solutions, exemplified by the use of a tethered fixed station for power transfer to the UAV, thereby extending its flight time [26]. Typically, in these applications, the tether is maintained slack to streamline UAV control. However, a taut tether presents notable advantages, including improved flight stability, enhanced physical interaction with ground objects, and superior stabilization. Moreover, some studies have delved into tethered aerial vehicle scenarios employing nonlinear controllers and observers, with the tether length regulated by an actuated winch. However, these studies assumed a fixed two-dimensional plane for the quadcopter and tether, limiting their applicability to more realistic scenarios [27]. This methodology was subsequently expanded to address physical human-robot interaction (pHRI), introducing a model for a human connected to an aerial vehicle via a tether. The aerial vehicle, in this case, can guide the human by pulling them along a desired path through the tether. To enhance pHRI safety, an admittance-based controller strategy was employed to calculate the required interaction force for guiding the human [28].

The proposed system consists of a ground vehicle and a flying robot connected by a taut tether to create haptic interaction with an admittance-based controller. A leader-follower strategy is used for the joint control of two robots with a velocity estimation method to enhance the tracking capabilities of the follower. The contributions of our study are as follows: (1) The system is simple compared to target tracking quadcopter equipped with camera and gimbal systems or systems engaging in collaborative action through high-level communication channels. Through the tether between the robots, there is indirect communication between them. (2) The leader and follower roles of the robots change dynamically to increase the robustness of the system in an unpredictable environment. (3) We assess the performance of our approach using different metrics that are mostly employed for measuring social interaction among humans, extending their application to the realm of joint robot control.

2. Methodology

We considered a quadcopter tethered to a ground robot as shown in Figure 1a. First, modeling and control of the quadcopter (Figure 1b) and the ground robot (Figure 1c) are introduced. Next, the tether model between the two robots is presented. Lastly, the admittance controller, which creates the compliant motion between the leader and follower robots, is discussed.

2.1. Modeling and control of the quadcopter

Equations of motion of the six DOF quadcopter connected to the ground robot are derived using Newton's equation of motion for the translational and rotational dynamics with the following assumptions: (1) Quadcopter

is considered as a rigid body, and its mass distribution is symmetrical, and its propellers are rigid, (2) The center of gravity and body-fixed reference frame coincide. (3) Earth's gravitational field, the mass of the quadcopter and body inertia matrix, the thrust factor, and the torque motor factors are constant. (4) The effects of aerodynamic drag forces are neglected. The quadcopter is considered to have a mass of m_1 , whereas the ground robot has a mass of m_2 . One end of the tether is attached to the center of mass of the quadcopter while the other end is connected to the center of mass of the ground robot, see Figure 1a. The tether is assumed to be taut with a length of l_0 . The tether is modeled as an elastic element with stiffness, k_c , and a weight of zero.

$$\ddot{\Phi} = \dot{\Theta}\dot{\Psi}\frac{I_y - I_z}{I_x} + \frac{1}{I_x}U_2, \quad (1)$$

$$\ddot{\Theta} = \dot{\Phi}\dot{\Psi}\frac{I_z - I_x}{I_y} + \frac{1}{I_y}U_3, \quad (2)$$

$$\ddot{\Psi} = \dot{\Phi}\dot{\Theta}\frac{I_x - I_y}{I_z} + \frac{1}{I_z}U_4, \quad (3)$$

$$\ddot{x} = (\cos\Phi\sin\Theta\cos\Psi + \sin\Phi\sin\Psi)\frac{1}{m_1}U_1 + \frac{1}{m_1}F_{Dx}, \quad (4)$$

$$\ddot{y} = (\cos\Phi\sin\Theta\sin\Psi - \sin\Phi\sin\Psi)\frac{1}{m_1}U_1 + \frac{1}{m_1}F_{Dy}, \quad (5)$$

$$\ddot{z} = (\cos\Phi\cos\Theta)\frac{1}{m_1}U_1 - g + \frac{1}{m_1}F_{Dz}, \quad (6)$$

where Φ , Θ , and Ψ are Euler angles (roll, pitch, and yaw, respectively), I_x , I_y , I_z are body inertia in x, y, z directions, respectively. U_1 is the total thrust force generated by the propellers (1st control input), U_2 is the roll moment generated by the left and right propellers (2nd control input), U_3 is the pitch moment generated by front and rear propellers (3rd control input), U_4 is the yaw torque generated by propellers (4th control input), and g is the gravitational acceleration of the Earth. F_{Dx} , F_{Dy} , and F_{Dz} are the interaction forces due to the tether connection. The rotor configuration, force, and moments generated by propellers and the reference frames are shown in Figure 1b. C is the origin of the body-fixed frame and $(xyz)_B$ is the body-fixed reference frame. The distance from the rotor axis to the body-fixed frame origin is l . Force generated by the i th rotor is F_i . O is the center of the inertial frame and $(xyz)_I$ is the inertial reference frame. The state and input vectors are given as follows:

$$\text{State vector} = x = [\Phi \ \dot{\Phi} \ \Theta \ \dot{\Theta} \ \Psi \ \dot{\Psi} \ x \ \dot{x} \ y \ \dot{y} \ z \ \dot{z}]^T, \quad (7)$$

$$\text{Input vector} = u = [U_1 \ U_2 \ U_3 \ U_4 \ F_{Dx} \ F_{Dy} \ F_{Dz}]^T. \quad (8)$$

The linearization of the state-space model is performed about the origin by using the nominal input vector given as

$$\text{Nominal state vector} : x_n = [0 \ 0 \ 0 \ 0 \ 0 \ 0 \ 0 \ 0 \ 0 \ 0 \ 0]^T, \quad (9)$$

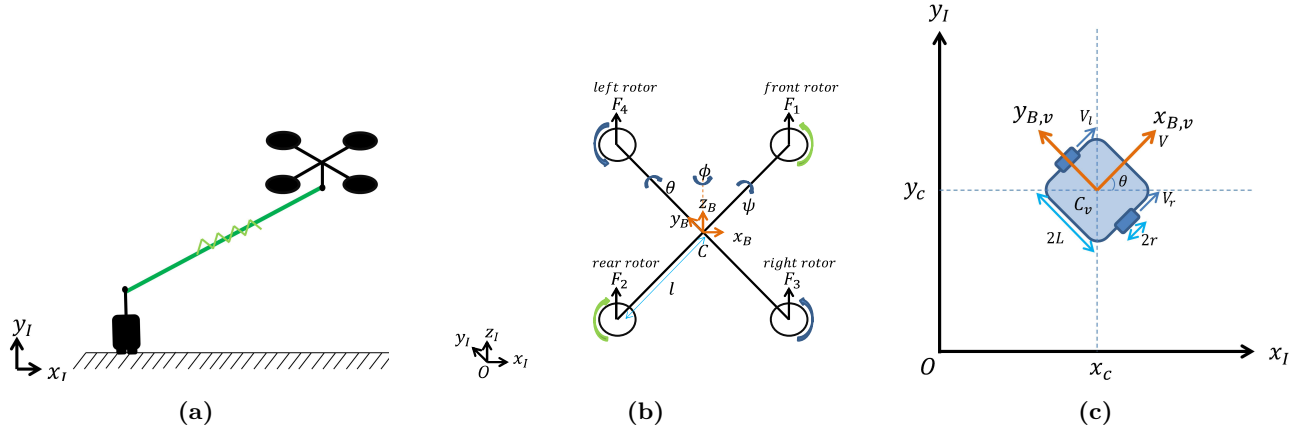


Figure 1. (a) Quadcopter and ground robot collaboration–tethered quadcopter. (b) Rotor configuration, force, and moments generated by propellers and reference frames of the quadcopter. (c) The velocities, heading, and reference frames of the ground robot in 2D.

$$\text{Nominal input vector : } u_n = [mg \ 0 \ 0 \ 0 \ 0 \ 0]^T. \quad (10)$$

The nonlinear state equations are given as f .

$$\dot{x} = f \quad (11)$$

The linearization is performed as follows:

$$\partial \dot{x} = \frac{\partial f}{\partial x_n} \partial x + \frac{\partial f}{\partial u_n} \partial u, \quad (12)$$

$$A = \frac{\partial f}{\partial x_n} \quad \text{and} \quad B = \frac{\partial f}{\partial u_n}, \quad (13)$$

$$\dot{x} = Ax + Bu. \quad (14)$$

B matrix is composed of B_m and B_D , which represent the input matrices for the manipulated input, u_m , and interaction force input u_D , respectively.

$$B = [B_m \ B_D]^T \quad (15)$$

The manipulated input vector, u_m , is composed of the thrust forces, U_1, U_2, U_3, U_4 .

$$u_m = [U_1 \ U_2 \ U_3 \ U_4]^T \quad (16)$$

The interaction forces are F_{Dx}, F_{Dy} , and F_{Dz} , which are shown in the vector u_D .

$$u_D = [F_{Dx} \ F_{Dy} \ F_{Dz}]^T \quad (17)$$

The controllability of the systems is presented by the rank of the controllability matrices of the linearized systems using the (A, B_m) pair. The controllability matrix is defined as follows:

$$C = [B_m \dots A^{11} B_m]. \tag{18}$$

The system is controllable, as shown by the rank of the controllability matrix. The system’s output comprises the flying robot’s position component on the x , y , and z directions, denoted by X , Y , and Z , respectively. The control system of the quadcopter is based on the state-feedback tracking controller as the inner loop of the control system and an admittance controller as the outer loop when it is considered as the follower robot. The control architecture is illustrated in Figure 2. The details of the admittance controller are discussed in subsection 2.4.

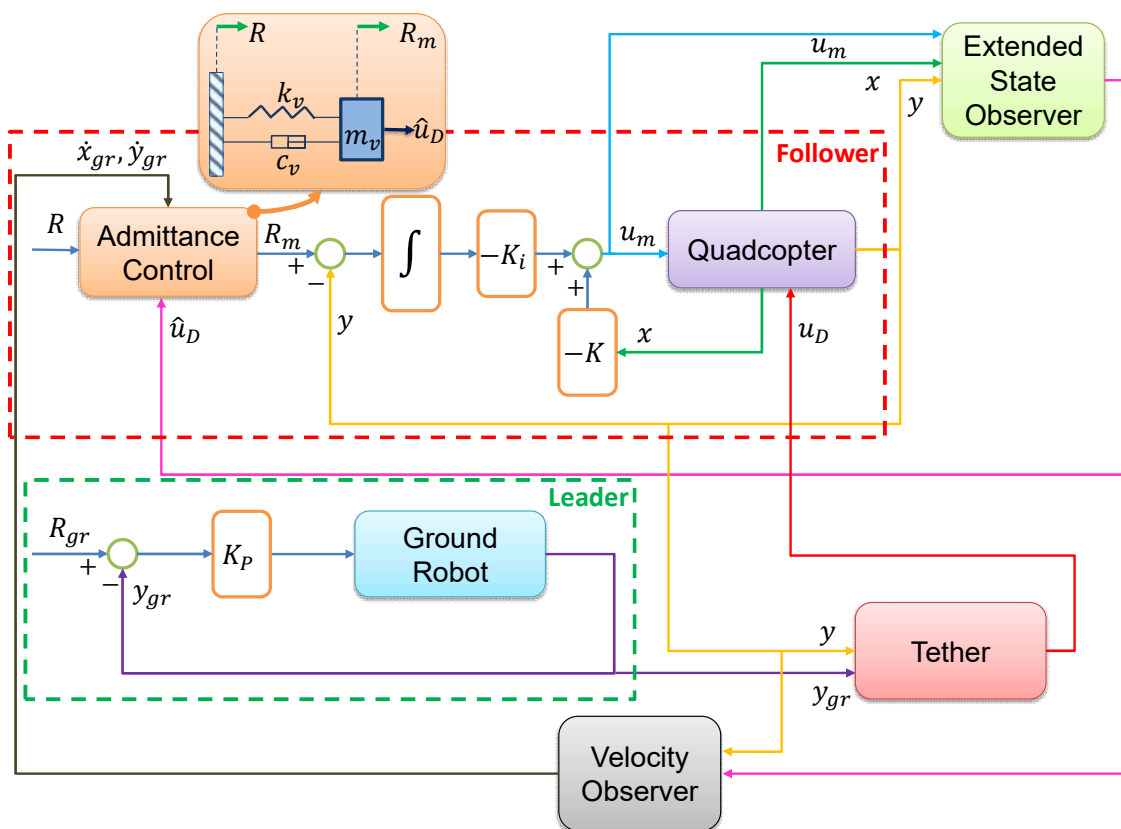


Figure 2. Control architecture when the quadcopter is the follower. The predefined trajectory of the ground robot is modified by the admittance controller according to the estimate of the force and velocity to feed the quadcopter.

The tracking control system is designed as a linear quadratic regulator (LQR). LQR is an optimum control strategy that minimizes a quadratic cost function, J .

$$J = \int_0^\infty x^T Q x + u^T R u dt, \tag{19}$$

where Q (size $n \times n$, n is the number of the states) and R (size $m \times m$, m is the number of inputs) are positive definitive symmetric matrices. Furthermore, integral feedback can be applied to LQR to increase control performance by decreasing steady-state error.

$$\bar{x} = \begin{bmatrix} x \\ \int_0^t e(\tau) d\tau, \end{bmatrix} \tag{20}$$

where $e = [R_X - X \ R_Y - Y \ R_Z - Z]^T$.

$$u_m = -[K \ K_I]\bar{x} \tag{21}$$

The extended state-space model is given as

$$\dot{\bar{x}} = \bar{A}\bar{x} + \bar{B}u_m + \begin{bmatrix} O_{12 \times 3} \\ I_{3 \times 3} \end{bmatrix} \begin{bmatrix} R_X \\ R_Y \\ R_Z \end{bmatrix}, \tag{22}$$

$$Y = [X \ Y \ Z]^T = C\bar{x}_k, \tag{23}$$

where $C = \begin{bmatrix} 0 & 0 & 0 & 0 & 0 & 0 & 1 & 0 & 0 & 0 & 0 & 0 \\ 0 & 0 & 0 & 0 & 0 & 0 & 0 & 0 & 1 & 0 & 0 & 0 \\ 0 & 0 & 0 & 0 & 0 & 0 & 0 & 0 & 0 & 0 & 1 & 0 \end{bmatrix}$.

\bar{A} and \bar{B} are defined as

$$\bar{A} = \begin{bmatrix} A & O_{12 \times 3} \\ -C & O_{3 \times 3} \end{bmatrix}, \tag{24}$$

$$\bar{B} = \begin{bmatrix} B \\ O_{3 \times 4} \end{bmatrix}. \tag{25}$$

Interaction vector u_D is observed by using an extended state-space model that includes F_{Dx} , F_{Dy} , and F_{Dz} as extended state variables. It is assumed that the time rate of change of the interaction forces is zero, leading to zero as state equations. The extended state vector and state equations are given as

$$\text{State vector} = x = [\Phi \ \dot{\Phi} \ \Theta \ \dot{\Theta} \ \Psi \ \dot{\Psi} \ x \ \dot{x} \ y \ \dot{y} \ z \ \dot{z} \ F_{Dx} \ F_{Dy} \ F_{Dz}]^T, \tag{26}$$

$$\dot{x}_o = [f \ O_{3 \times 1}]^T. \tag{27}$$

An observer is designed based on the linearized dynamical model of the observer. The linearization is performed as

$$\partial \dot{x}_o = \frac{\partial f_o}{\partial x_o} \partial x_o + \frac{\partial f}{\partial u_m} \partial u_m, \tag{28}$$

$$A_o = \frac{\partial f_o}{\partial x_o} \quad \text{and} \quad B_o = \frac{\partial f}{\partial u_m}, \tag{29}$$

$$\dot{x}_o = A_o x_o + B_o u_m. \tag{30}$$

The nominal state vector and input vector are given as

$$\text{Nominal state vector} : x_n = [0 \ 0 \ 0 \ 0 \ 0 \ 0 \ 0 \ 0 \ 0 \ 0 \ 0 \ 0 \ 0 \ 0 \ 0]^T, \tag{31}$$

$$\text{Nominal input vector : } u_n = [mg \ 0 \ 0 \ 0]^T. \quad (32)$$

The measurement vector, y_o is given as

$$y_o = C_o x_o, \quad (33)$$

where $C_o = [I_{12 \times 12} \ O_{12 \times 3}]^T$.

The observability analysis is performed using the (A_o, B_m) pair. The observability matrix, \mathcal{O} , is given as

$$\mathcal{O} = [C_o \ \dots \ C_o A_o^{14}]^T. \quad (34)$$

It is shown that the rank of the observability matrix is 15. Therefore, using the aforementioned model, an observer is designed to estimate the interaction forces $\hat{u}_D = [\hat{F}_{Dx} \ \hat{F}_{Dy} \ \hat{F}_{Dz}]^T$. The observer dynamics are presented as

$$\hat{x}_o = A_o \hat{x}_o + B_o u_m + L_o (y - C_o x_o). \quad (35)$$

The observer gain matrix, L_o , is determined using the pole placement technique so that the observer dynamic is faster than the closed-loop system tracking control dynamic. It is assumed that these interaction forces have an influence on the quadcopter dynamics while the motion of the ground robot is not affected.

2.2. Modeling and control of the ground robot

The ground robot is modeled as a differential drive robot. Its velocity and orientation are controlled for maneuvering. C_v is the body-fixed frame origin of the ground robot shown in Figure 1c, and $(xy)_{B,v}$ is the body-fixed reference frame of the ground robot. O is the center of the inertial frame and $(xy)_I$ is the inertial reference frame. The distance between the center of the wheels is $2L$. The radius of the wheel is r . The velocities of the right and left wheels are V_r and V_l , respectively, and V is the linear velocity. The orientation of the ground robot is Θ_v . The dynamical equations of the ground robot are derived with the following assumptions: the wheels of the robot do not slip, and the surface is flat. The duration of the robot's motion is within a short period; therefore, the right and left wheel velocities are constant during that duration and the robot is moving with a constant velocity. The equations of motion are as follows:

$$\dot{x}_{c,B,v} = V \cos \Theta, \quad (36)$$

$$\dot{y}_{c,B,v} = V \sin \Theta, \quad (37)$$

$$\dot{\Theta} = \frac{V_r - V_l}{2L}, \quad (38)$$

where $\dot{x}_{c,B,v}$ and $\dot{y}_{c,B,v}$ are the rate of change of the position of the ground robot in x and y directions, respectively, and $\dot{\Theta}$ is the angular velocity of the ground robot. The control system of the ground robot is based on a proportional controller in the inner control loop and if it is the follower robot, an admittance controller is in the outer control loop. The control architecture for the case where the ground robot is the follower robot is given in Figure 3. The details of the admittance controller are discussed in subsection 2.4.

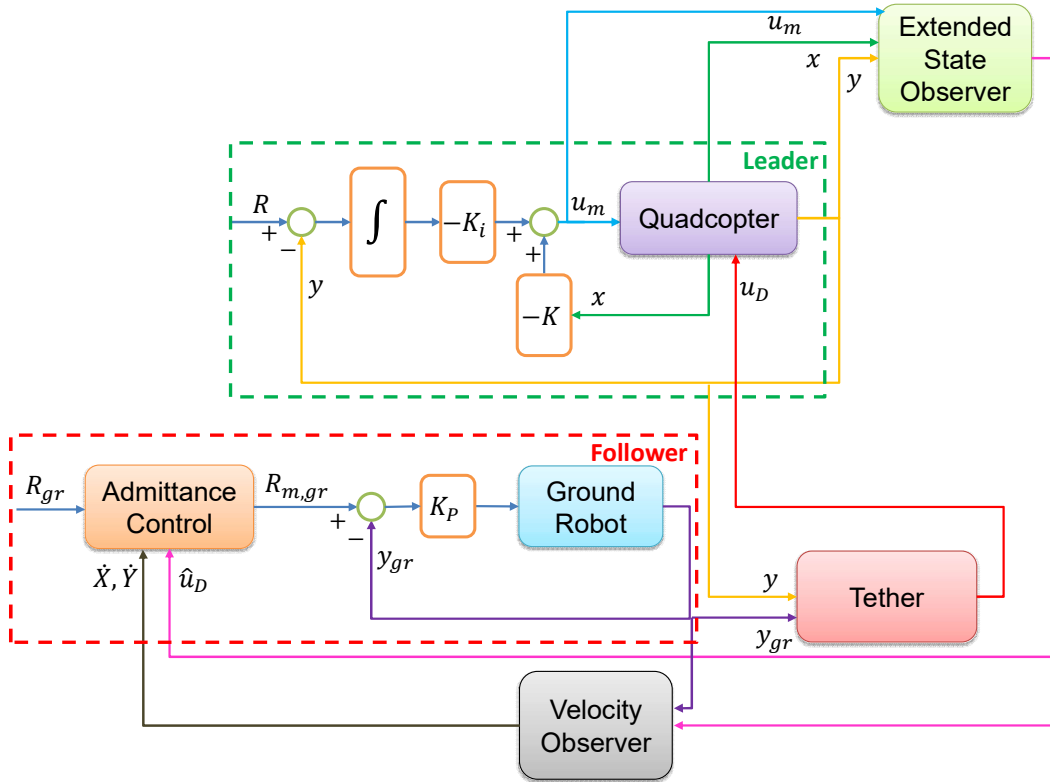


Figure 3. Control architecture when the ground robot is the follower. The predefined trajectory of the quadcopter is modified by the admittance controller according to the estimate of the force and velocity to feed the ground robot.

2.3. Tether model

The model we use for the tether is a spring model that eliminates the assumption of inelastic collisions [29]. The spring only generates a force when the tether length is equal to or greater than its unstretched length. Otherwise, if the tether length is less than the unstretched length, the tether is slack, and the tension is zero. Hence, there is no interaction between the quadcopter and the ground robot. Assuming that the tether is taut, we get the following relation:

$$F_t = \begin{cases} k_c(l_{cable} - l_0) & \text{if } l_{cable} \geq l_0 \\ 0 & \text{otherwise} \end{cases} \quad (39)$$

F_t is the overall tension on the tether. k_c is the stiffness coefficient of the tether. l_{cable} is the stretched tether length and l_0 is the unstretched tether length. The forces in the x , y , and z directions are found by using trigonometric relations.

2.4. Admittance controller for the follower robot

An admittance controller is designed for the follower robot. The admittance controller modifies the reference input by using the virtual mass-spring-damper system that is driven by the estimated interaction forces \hat{F}_{Dx} and \hat{F}_{Dy} . In other words, the admittance controller takes the force as an input and gives the displacement as an output to control the position of the follower robot. It is important to note that the leader robot follows the

trajectory given as a reference, while the admittance controller generates the trajectory of the follower robot in x and y directions.

$$m_v \ddot{R}_X + b_v \dot{R}_X + k_v R_X = b_v \dot{X}_D + k_v X_D + \hat{F}_{Dx} \quad (40)$$

$$m_v \ddot{R}_Y + b_v \dot{R}_Y + k_v R_Y = b_v \dot{Y}_D + k_v Y_D + \hat{F}_{Dy} \quad (41)$$

The tracking control system is depicted in Figure 2 for the case where the quadcopter is the follower. R includes reference position in z - direction while trajectory in x - and y - directions are created according to the observed forces. There is no direct trajectory information for the follower robot. R_{gr} is the vector of the reference input of the ground robot.

$$R = [R_Z]^T \quad (42)$$

$$R_{gr} = [R_{\dot{X}} \ R_{\dot{Y}} \ R_{\Theta}]^T \quad (43)$$

R_m is the modified reference input manipulated by the admittance controller.

$$R_m = [R_{m,\dot{X}} \ R_{m,\dot{X}}]^T \quad (44)$$

The tracking control system for the case where the ground robot is the follower is depicted in Figure 3. R is the vector of the reference input of the quadcopter, and R_{gr} includes the heading of the ground robot taken directly from the quadcopter heading information while the trajectory in x and y directions are created according to the observed interaction forces.

$$R = [R_X \ R_Y \ R_Z]^T \quad (45)$$

$$R_{gr} = [R_{\Theta}]^T \quad (46)$$

$R_{m,gr}$ is the modified reference input manipulated by the admittance controller.

$$R_{m,gr} = [R_{m,\dot{X}_{gr}} \ R_{m,\dot{Y}_{gr}}]^T \quad (47)$$

The admittance controller regulates the motion of the follower robot based on the observed interaction force as discussed before. The velocity input is set to zero to ensure that the follower robot maintains its position as long as there is no interaction force. This approach, however, results in a steady-state error between the leader and follower robots. As a result, we developed a velocity estimator without using additional sensor data. The estimation model is inspired by Takagi et al. [30]. They created an interactive learning paradigm by using a dual robot system connected physically. They showed that the haptic forces between the robots can be used to estimate the targets of each robot. Similarly, we created a model in which the follower robot can estimate the velocity of the leader through the interaction forces and use this information to improve its tracking ability.

$$\tilde{x} \approx F/k_c + x, \quad (48)$$

where \tilde{x} are the state of the follower robot, F is the interaction force between them, and k_c is the stiffness coefficient of the tether.

3. Experimental analysis

In this section, we present the implementation of our method in the MATLAB/Simulink environment. Later, we introduce the metrics used to evaluate the performance of our method.

3.1. Experimental setup

First, the six DOF equations of motion for the quadcopter with motor dynamics are implemented using MATLAB/Simulink. Next, an LQR controller is designed for the leader to track the reference trajectory. The selection of the weighting matrices, Q and R , plays a crucial role in the LQR design, as poorly chosen values can lead to inaccurate tracking or even motion instabilities. However, deriving the matrices analytically is challenging due to their implicit dependencies between elements. Therefore, empirical values were chosen for $Q = [1 \ 1 \ 1 \ 1 \ 1 \ 1 \ 1 \ 1 \ 1 \ 1]$ and $R = [0.1 \ 0.1 \ 0.1 \ 0.1]$ identity matrix. Subsequently, the optimal gain matrix, K , is calculated using the LQR function in MATLAB. In addition, the dynamic model of the ground robot is implemented in MATLAB/Simulink, and its velocity and orientation are controlled by a proportional controller with a gain of 2. The physical parameters of the quadcopter and ground robot used in the simulation are listed in Table 1.

Table 1. Physical parameters of the quadcopter and ground robot [28].

Parameters	Definition	Value	Unit
m	Mass of the quadcopter	1	kg
g	Gravitational acceleration	9.81	m/s^2
l	Distance between COG and rotor center	0.35	m
b	Trust coefficient	0.001	-
d	Drag coefficient	0.001	-
I_{xx}, I_{yy}, I_{zz}	Body inertia in x, y, z directions	0.1402	kgm^2
L	Distance between COG and wheel center	0.2	m

Furthermore, we need to implement the interaction forces due to the tether between the two robots. The tether is implemented as a linear spring in the simulations. The spring constant is calculated as 25 N/m using $A_c = \pi(\frac{d_c}{2})^2$ and $k_c = \frac{EA_c}{l_c}$ with the parameters: $d_c = 10^{-3} \text{ m}$, $l_c = 6 \text{ m}$, and $E = 194.10 \text{ MPa}$. As discussed previously, in the simulations, we assume that the tether is taut so that there is always a tension force between the quadcopter and ground robots. The tension forces are observed with an observer and used in the admittance controller. The nominal values of the admittance controller parameters are taken as 0.0002 N/m for k_v , 0.1 kg for m_v , and 3 Ns/m for c_v .

3.2. Metrics

Different metrics are used in different experiments. In Monte Carlo simulations and validation experiments, as discussed in Section 4, RMS of position error and circular variance (CV) metrics are used. In transient response experiments, standard metrics such as settling time and maximum percent overshoot are used to assess the transient response characteristics. The RMS of position error is calculated as

$$e_p = \sqrt{\frac{1}{n} \sum_{k=1}^n (x_{1,k} - x_{2,k})^2}, \quad (49)$$

where n is the number of time steps in the simulation, and $x_{1,k}$ and $x_{2,k}$ show the positions of the leader and follower robots at the k_{th} time step, respectively. The CV metric is used to quantify the coordination level between agents. In particular, we used the index based on circular variance to measure the phase synchronization index [31–33] and calculated it as

$$CV = \left\| \frac{1}{n} \sum_{j=1}^n \exp(i\Delta\phi_j) \right\|, \quad (50)$$

where the circular variance of the angular distribution is obtained by transforming the phase difference into the unit circle in the complex plane. $\Delta\phi_j$ is the relative phase between the leader and the follower robots at j_{th} time step, n represents the total number of time steps. The index of phase synchronization is bound to the range $[0, 1]$. Values close to 0 indicate no phase synchronization, whereas values close to 1 show a higher coordination level between the robots.

4. Results and discussion

This section is divided into four subsections that describe how to implement the suggested joint control approach, beginning with a basic test trajectory that uses nominal values for admittance controller parameters, followed by a comparative result from the existing literature. The method for fine-tuning these settings is then described. Before running the system through testing with a complicated trajectory, the transient responses are evaluated, as well. There are role exchanges in subsections 4.1, 4.3, and 4.5 and performance is compared with and without the use of velocity estimates in the control method. This section concludes with the complicated test performance.

4.1. Circular trajectory experiment

In this experiment, we test the trajectory-tracking performance of the follower and the leader robots. The nominal control parameters mentioned in subsection 3.1 are utilized. The robots are required to follow a circular trajectory for 100 s. In the first 50 s of the experiment, the quadcopter is the leader; in the last 50 s, the role of the robots changes. The trajectories of the quadcopter and the ground robot are depicted in Figure 4. In Figures 4a and 4c, the trajectories are plotted without velocity estimation, and Figures 4b and 4d is for with velocity estimation. Without velocity estimation, the follower cannot perfectly track the leader, and there is always a lag, as observed in the trajectory of the ground robot both in the x - and y - directions in the first half of the experiment. The same phenomenon is also observed in the last half of the experiment in the trajectory of the quadcopter as shown in Figure 4a. This is also evident in Figure 4c, where the trajectory of neither the leader nor the follower resembles a full circle. However, with velocity estimation, the follower tracks the leader with a minimal lag both in x - and y - directions as shown in Figure 4b, resulting in an almost perfect circular trajectory as shown in Figure 4d. This phenomenon is due to the change in the references of both robots during their role exchange at 50 s. In the first 50 s, since the quadcopter is the leader, it is given positional reference commands. It tracks the reference with minimal error during this period, as discussed previously. However, this is not the case for the ground robot. The position of the ground robot lags the quadcopter considerably since its reference is generated by the admittance controller that already lags the positional reference command of the quadcopter as in Figure 4a. At 50 s, since the quadcopter becomes the follower, its reference is created by the admittance controller based on the position of the ground robot, causing a jump in its position that is shown in Figure 4c.

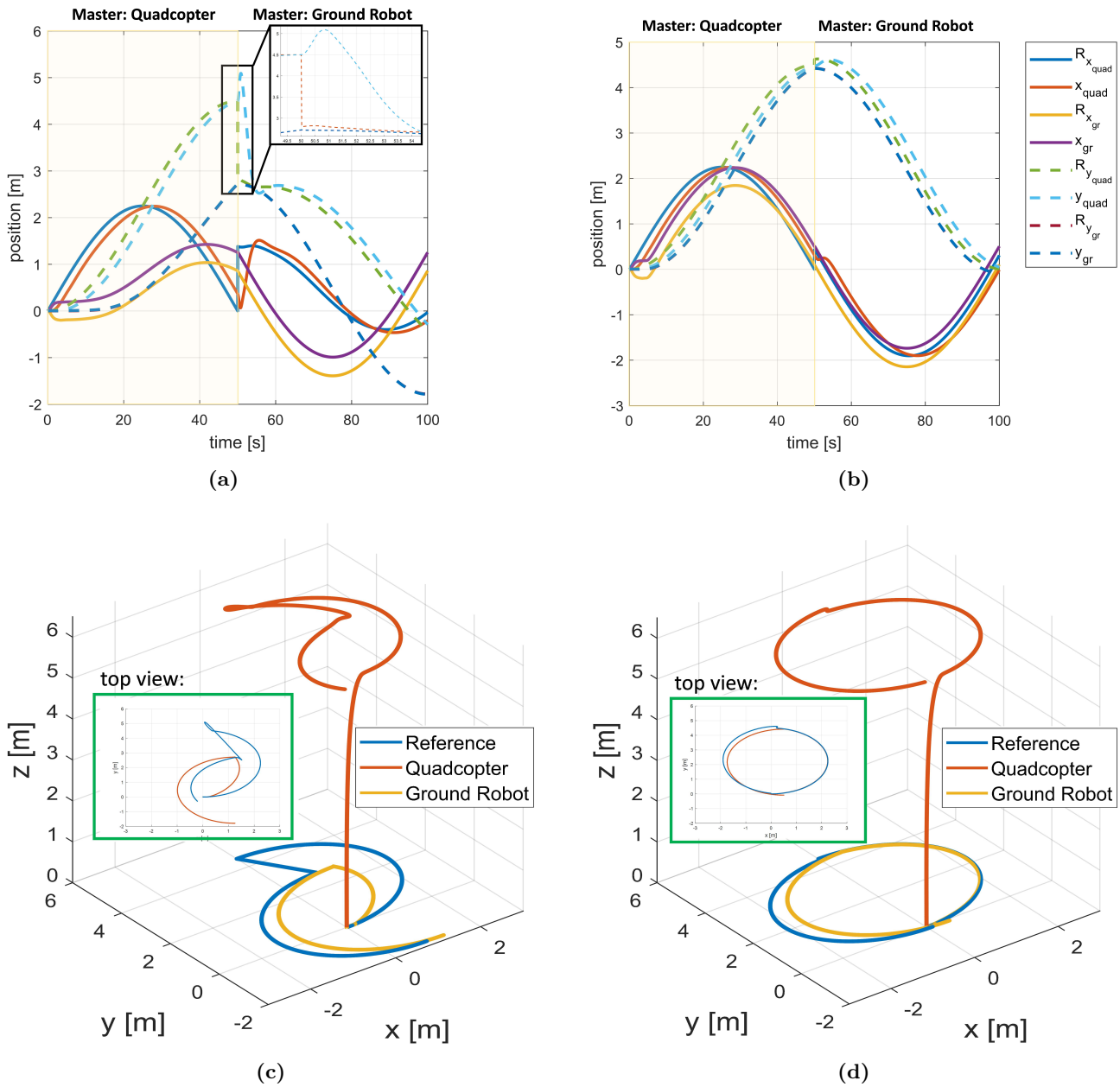


Figure 4. Dynamic role exchange experiments with linear trajectories with circular trajectories. (a) Positions without velocity estimation, inset shows the zoomed version of the positions. (b) Positions with velocity estimation. The solid line shows the movement in the x -direction, and the dashed line shows the movement in the y -direction. $R_{x,quad}$, $R_{y,quad}$ and $R_{x,gr}$, $R_{y,gr}$ represent reference trajectories for quadcopter and ground robot, respectively. x_{quad} and y_{quad} represent the trajectory of the quadcopter in both directions. x_{gr} and y_{gr} represent the trajectory of ground in both directions. (c) The 3D trajectory without velocity estimation. (d) The 3D trajectory with velocity estimation. In (c) and (d), insets show the top view of the trajectory.

4.2. Comparative experiment

In this experiment, we compared our approach with a similar method in the literature [28] that involves a quadcopter as the leader, and a human as the follower, navigating obstacles. Unlike our method, their control strategy also employs an admittance controller for the leader to adjust the tension so that it does not exceed human limits. We implemented this method in our framework and used a similar experimental setup as shown in Figure 5a. The ground robot with velocity estimation tracks the leader almost without any error and without velocity estimation, it lags the leader. The ground robot with the method in [28] performs better than the latter method but does not achieve the performance of the former method. We compare our model with the one proposed in the literature using the metrics; root mean square (RMS) of position error and coefficient of variation (CV), as presented in Table 2.

Table 2. The metric results comparison of our proposed model and method in [28].

Metric	w. vel. est.	w/o vel. est.	met. in [28]
RMS	0.43	1.03	0.96
CV	0.98	0.68	0.71

The time evolution of its position is depicted in Figure 5b. Since the main motivation in [28] is to provide enough safety distance between the human and quadcopter, in a test with a ground robot, it introduces a lag deteriorating the tracking performance of the slave considerably.

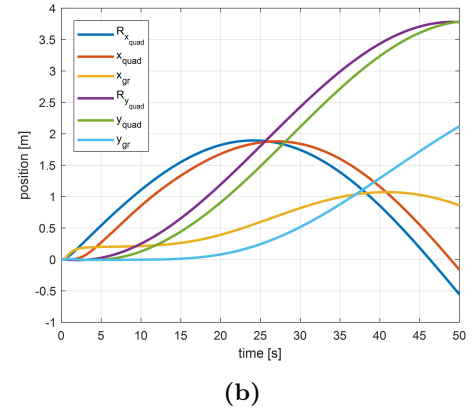
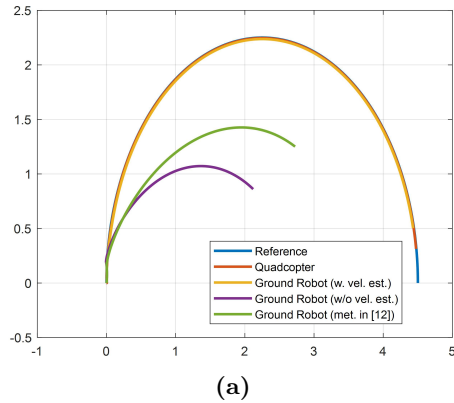


Figure 5. Comparative experiment. (a) Trajectories of the quadcopter (red), ground robot with velocity estimation (yellow), without velocity estimation (purple), and with the controller in [28] (green). (b) The evolution of the position of the ground robot with the latter method and the quadcopter. The nominal control parameters mentioned in subsection 3.1 are utilized.

4.3. Monte Carlo simulations

To fine-tune the admittance controller parameters in our proposed system, we utilize Monte Carlo simulations. In these experiments, the leader and follower change roles dynamically in an arena with four obstacles placed on the ground, as shown in Figure 6a. The course is 75 m long, and each obstacle is 15 m apart. During the experiment, the quadcopter is flying 6 m above the ground robot. k_v is set to 0.002 N/m to guarantee full

compliance with the interaction force [34]. In order to find the optimal set of parameters, m_v and c_v are set in range [5, 25] kg and [5, 25] Ns/m, respectively. Each value is incremented by one and simulations are repeated three times for each setting. The quadcopter starts the experiment as the leader and stays as the leader till the ground robot detects an obstacle. During obstacle avoidance, the ground robot stays as the leader, and then the roles exchange till the next obstacle. In this way, the roles exchange nine times in a single run. Results, shown in Figures 6b and 6c, and indicate that selecting parameters in certain regions (dark blue) improves accuracy (RMS metric) and synchronization (bright yellow) (CV metric). Overall, these results show that there is a feasible region to select for m_v and c_v for better performance.

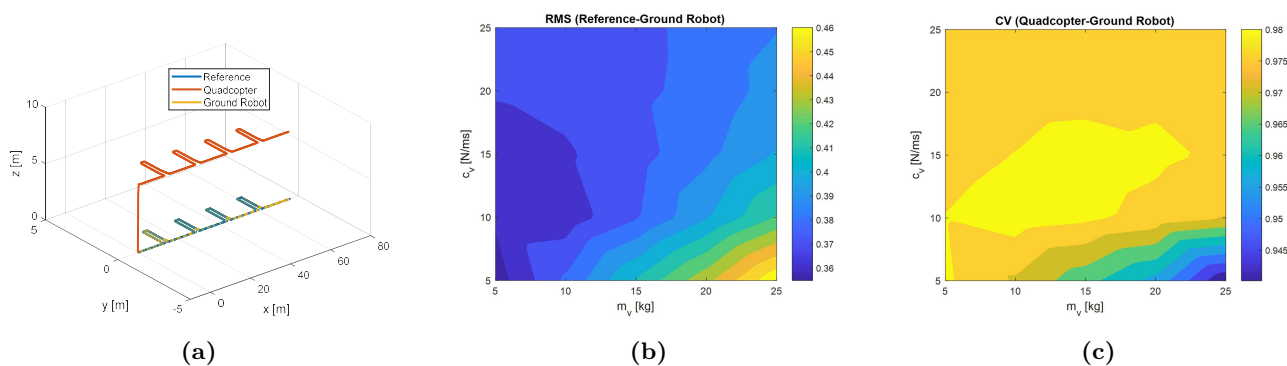


Figure 6. Dynamic role exchange experiments with a linear trajectory. (a) The 3D trajectory, (b) the RMS of position error, and (c) the CV between the quadcopter and the ground robot.

4.4. Transient response experiments

Based on the results of the Monte Carlo simulations, we have identified a feasible range for the admittance controller parameters. We utilized these selected parameters to analyze their impact on the transient response of the system, using both the rise time and maximum overshoot. In the experiments, the ground robot moves as the leader robot with a constant velocity of 0.1 m/s. We terminated the experiment once the ground robot had moved a distance of 15 m. During the experiment, the quadcopter was flying 6 m above the ground robot. We repeated each controller parameter experiment three times, and the mean values are depicted in Figure 7a. We have chosen 5 kg and 15 Ns/m for m_v and c_v , respectively, to achieve the shortest rise time (1.65 s) and an acceptable percentage overshoot (10.51%).

4.5. Validation experiments

In this experiment, we apply our method in a complex scenario, initially with the quadcopter as the leader following a square path, then switching to the ground robot as the leader following a circular path. The robot maneuvers in the x - direction, avoiding an obstacle, and later turns 90° to move in the y - direction, avoiding another obstacle. Results are shown in Figures 7b and 7c. With velocity estimation, the follower tracks the leader with minimal error, evident in reduced RMS and CV metrics (0.388 and 0.956). However, without velocity estimation, significant lag occurs, reflected in higher metrics (1.069 and 0.840). Incorporating predicted velocity in the control system improves synchronization leading to smoother movement and resembling harmonious dynamics observed in biological systems such as human-human haptic interaction [35].

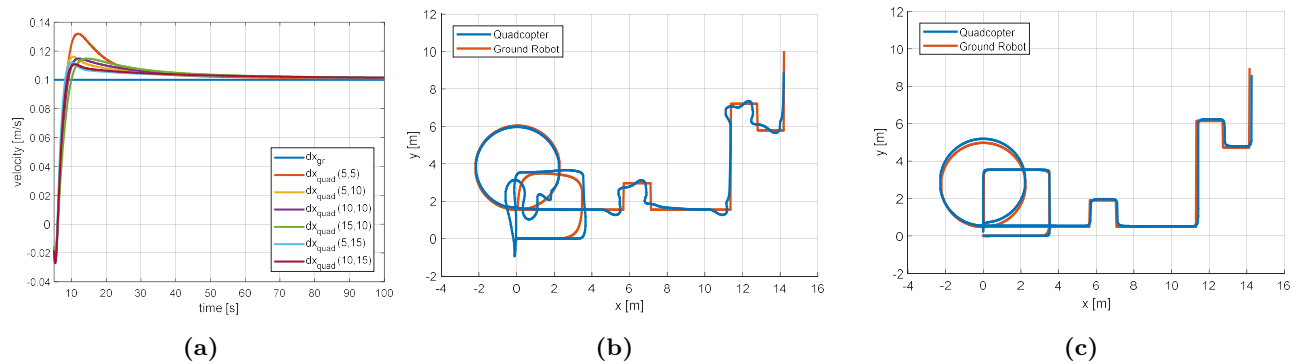


Figure 7. (a) Transient response analysis where the ground robot moves with a constant velocity as master, (b) the validation experiment. The blue line shows the quadcopter movement and the red line stands for ground robot movement, without velocity estimation, (c) with velocity estimation.

5. Conclusion

This study introduces a leader-follower control framework for a quadcopter and ground robot. It utilizes an admittance-based controller with an extended state observer for tether force estimation and a velocity estimator to improve the follower robot's tracking performance. To optimize the proposed control system, a thorough exploration of virtual controller parameters is conducted through Monte Carlo analysis, with a focus on metrics such as the RMS of position error and CV. Transient analysis refines the virtual admittance controller parameters. Finally, we validated the robustness of our approach through various simulation-based experiments in the MATLAB/Simulink environment. Future work involves applying and validating the method with real robots in realistic scenarios.

References

- [1] Altan A. Performance of metaheuristic optimization algorithms based on swarm intelligence in attitude and altitude control of unmanned aerial vehicle for path following. In: IEEE 2020 4th International Symposium on Multidisciplinary Studies and Innovative Technologies; İstanbul, Türkiye; 2020. pp. 1-6. <https://doi.org/10.1109/ISMSIT50672.2020.9255181>
- [2] Belge E, Altan A, Hacıoğlu R. Metaheuristic optimization-based path planning and tracking of quadcopter for payload hold-release mission. *Electronics* 2022; 11 (8): 1208. <https://doi.org/10.3390/electronics11081208>
- [3] Altan A, Hacıoğlu R. Model predictive control of three-axis gimbal system mounted on UAV for real-time target tracking under external disturbances. *Mechanical Systems and Signal Processing* 2020; 138: 106548. <https://doi.org/10.1016/j.ymssp.2019.106548>
- [4] Wang Y, Qi R, He C. Trajectory and attitude cooperative formation control for air-ground collaborative systems under communication faults. In: IEEE 2023 6th International Symposium on Autonomous Systems; Nanjing, China; 2023. pp. 1-6. <https://doi.org/10.1109/ISAS59543.2023.10164619>
- [5] Mellinger D, Lindsey Q, Shomin M, Kumar V. Design, modeling, estimation and control for aerial grasping and manipulation. In: 2011 IEEE/RSJ International Conference on Intelligent Robots and Systems; San Francisco, CA, USA; 2011. pp. 2668-2673. <https://doi.org/10.1109/IROS.2011.6094871>
- [6] Palunko I, Cruz P, Fierro R. Agile load transportation: safe and efficient load manipulation with aerial robots. *IEEE Robotics and Automation Magazine* 2012; 19 (3): 69-79. <https://doi.org/10.1109/MRA.2012.2205617>

- [7] Sreenath K, Michael N, Kumar V. Trajectory generation and control of a quadrotor with a cable-suspended load-a differentially-flat hybrid system. In: 2013 IEEE International Conference on Robotics and Automation; Karlsruhe, Germany; 2013. pp. 4888-4895. <https://doi.org/10.1109/ICRA.2013.6631275>
- [8] Faust A, Palunko I, Cruz P, Fierro R, Tapia L. Learning swing-free trajectories for UAVs with a suspended load. In: 2013 IEEE International Conference on Robotics and Automation; Karlsruhe, Germany; 2013. pp. 4902-4909. <https://doi.org/10.1109/ICRA.2013.6631277>
- [9] Goodarzi FA, Lee D, Lee T. Geometric stabilization of a quadrotor UAV with a payload connected by flexible cable. In: 2014 American Control Conference; Portland, OR, USA; 2014. pp. 4925-4930. <https://doi.org/10.1109/ACC.2014.6859419>
- [10] Alaimo A, Artale V, Milazzo C, Ricciardello A, Trefiletti L. Mathematical modeling and control of a hexacopter. In: 2013 International Conference on Unmanned Aircraft Systems (ICUAS); Atlanta, GA, USA; 2013. pp. 1043-1050. <https://doi.org/10.1109/ICUAS.2013.6564793>
- [11] Sreenath K, Kumar V. Dynamics, control and planning for cooperative manipulation of payloads suspended by cables from multiple quadrotor robots. *Robotics: Science and Systems 2013*. <https://doi.org/10.15607/RSS.2013.IX.011>
- [12] Michael N, Fink J, Kumar V. Cooperative manipulation and transportation with aerial robots. *Autonomous Robots* 2011; 30: 73-86. <https://doi.org/10.1007/s10514-010-9205-0>
- [13] Mellinger D, Shomin M, Michael N, Kumar V. Cooperative grasping and transport using multiple quadrotors. In: Martinoli A, Mondada F, Correll N, Mermoud G, Egerstedt M et al. (editors). *Distributed Autonomous Robotic Systems*. Springer Tracts in Advanced Robotics, Vol 83. Berlin, Germany: Springer, 2013. pp. 545-558. https://doi.org/10.1007/978-3-642-32723-0_39
- [14] Turpin M, Mohta K, Michael N, Kumar V. Goal assignment and trajectory planning for large teams of interchangeable robots. *Autonomous Robots* 2014; 37 (4): 401-415. <https://doi.org/10.1007/s10514-014-9412-1>
- [15] Chen J, Sun D, Yang J, Chen H. Leader-follower formation control of multiple non-holonomic mobile robots incorporating a receding-horizon scheme. *The International Journal of Robotics Research* 2010; 29 (6): 727-747. <https://doi.org/10.1177/0278364909104290>
- [16] Fierro R, Das AK, Kumar V, Ostrowski JP. Hybrid control of formations of robots. In: *Proceedings 2001 ICRA. IEEE International Conference on Robotics and Automation*; Seoul, Korea (South); 2001. pp. 157-162. <https://doi.org/10.1109/ROBOT.2001.932546>
- [17] Mariottini G, Morbidi F, Prattichizzo D, Vander Valk N, Michael N et al. Vision-based localization for leader-follower formation control. *IEEE Transactions on Robotics* 2009; 25 (6): 1431-1438. <https://doi.org/10.1109/TRO.2009.2032975>
- [18] Lupashin S, D'Andrea R. Stabilization of a flying vehicle on a taut tether using inertial sensing. In: 2013 IEEE/RSJ International Conference on Intelligent Robots and Systems; Tokyo, Japan; 2013. p. 2432-2438. <https://doi.org/10.1109/IROS.2013.6696698>
- [19] Kiribayashi S, Yakushigawa K, Nagatani K. Design and development of tether-powered multirotor micro unmanned aerial vehicle system for remote-controlled construction machine. In: Hutter M, Siegwart R (editors). *Field and Service Robotics*. Springer Proceedings in Advanced Robotics, vol 5. Cham, Switzerland: Springer, 2018. pp. 637-648. https://doi.org/10.1007/978-3-319-67361-5_41
- [20] Nicotra MM, Naldi R, Garone E. Taut cable control of a tethered UAV. *IFAC Proceedings Volumes* 2014; 47 (3): 3190-3195. <https://doi.org/10.3182/20140824-6-ZA-1003.02581>
- [21] Tognon M, Franchi A. Nonlinear observer-based tracking control of link stress and elevation for a tethered aerial robot using inertial-only measurements. In: 2015 IEEE International Conference on Robotics and Automation (ICRA); Seattle, WA, USA; 2015. pp. 3994-3999. <https://doi.org/10.1109/ICRA.2015.7139757>

- [22] Tognon M, Franchi A. Nonlinear observer for the control of bi-tethered multi aerial robots. In: 2015 IEEE/RSJ International Conference on Intelligent Robots and Systems; Hamburg, Germany; 2015. pp. 1852-1857. <https://doi.org/10.1109/IROS.2015.7353619>
- [23] Sandino LA, Bejar M, Kondak K, Ollero A. Advances in modeling and control of tethered unmanned helicopters to enhance hovering performance. *Journal of Intelligent and Robotic Systems* 2014; 73: 3-18. <https://doi.org/10.1007/s10846-013-9910-y>
- [24] Oh SR, Pathak K, Agrawal SK, Pota HR, Garratt M. Approaches for a tether-guided landing of an autonomous helicopter. *IEEE Transactions on Robotics* 2006; 22 (3): 536-544. <https://doi.org/10.1109/TRO.2006.870657>
- [25] Sandino L, Santamaria D, Bejar M, Viguria A, Kondak K et al. Tether-guided landing of unmanned helicopters without GPS sensors. In: 2014 IEEE International Conference on Robotics and Automation; Hong Kong, China; 2014. pp. 3096-3101. <https://doi.org/10.1109/ICRA.2014.6907304>
- [26] Jain KP, Kotaru P, Desa M, Mueller MW, Sreenath K. Tethered power supply for quadcopters: architecture, analysis and experiments. *arXiv preprint 2022*; 2203.08180v1 [eess.SY]. <https://doi.org/10.48550/arXiv.2203.08180>
- [27] Tognon M, Dash SS, Franchi A. Observer based control of position and tension for an aerial robot tethered to a moving platform. *IEEE Robotics and Automation Letters* 2016; 1 (2):732-737. <https://doi.org/10.1109/LRA.2016.2523599>
- [28] Tognon M, Alami R, Siciliano B. Physical human-robot interaction with a tethered aerial vehicle: application to a force-based human guiding problem. *IEEE Transactions on Robotics* 2021; 37 (3): 723-734. <https://doi.org/10.1109/TRO.2020.3038700>
- [29] Lv N, Liu J, Xia H, Ma J, Yang X. A review of techniques for modeling flexible cables. *Computer-Aided Design* 2020; 122: 102826. <https://doi.org/10.1016/j.cad.2020.102826>
- [30] Börner H, Carboni G, Cheng X, Takagi A, Hirche S et al. Physically interacting humans regulate muscle coactivation to improve visuo-haptic perception. *Journal of Neurophysiology* 2022; 129 (2): 494-499. <https://doi.org/10.1152/jn.00420.2022>
- [31] Delaherche E, Chetouani M, Mahdhaoui A, Saint-Georges C, Viaux S et al. Interpersonal synchrony: a survey of evaluation methods across disciplines. *IEEE Transactions on Affective Computing* 2012; 3 (3): 49-365. <https://doi.org/10.1109/T-AFFC.2012.12>
- [32] Kreuz T, Mormann F, Andrzejak RG, Kraskov A, Lehnertz K et al. Measuring synchronization in coupled model systems: A comparison of different approaches. *Physica D: Nonlinear Phenomena* 2007; 225 (1): 29-42. <https://doi.org/10.1016/j.physd.2006.09.039>
- [33] Oullier O, DeGuzman GC, Jantzen KJ, Lagarde J, ScottKelso JA. Social coordination dynamics: measuring human bonding. *Social Neuroscience* 2008; 3 (2): 178-192. <https://doi.org/10.1080/17470910701563392>
- [34] Tagliabue A, Kamel M, Siegwart R, Nieto J. Robust collaborative object transportation using multiple MAVs. *The International Journal of Robotics Research* 2019; 38 (9): 1020-1044. <https://doi.org/10.1177/0278364919854131>
- [35] Takagi A, Hirashima M, Nozaki D, Burdet E. Individuals physically interacting in a group rapidly coordinate their movement by estimating the collective goal. *eLife* 2019; 8: e41328. <https://doi.org/10.7554/eLife.41328>